Ultrasound-Specific Segmentation via Decorrelation and Statistical Region-Based Active Contours

Greg Slabaugh, Gozde Unal, Tong Fang
Intelligent Vision and Reasoning Department
Siemens Corporate Research
Princeton, NJ USA
{greg.slabaugh,gozde.unal,tong.fang}@siemens.com

Michael Wels
Department of Computer Science
Universität Würzburg
Coburg, Germany
michael.wels@eliteakademie.de

Abstract

Segmentation of ultrasound images is often a very challenging task due to speckle noise that contaminates the image. It is well known that speckle noise exhibits an asymmetric distribution as well as significant spatial correlation. Since these attributes can be difficult to model, many previous ultrasound segmentation methods oversimplify the problem by assuming that the noise is white and/or Gaussian, resulting in generic approaches that are actually more suitable to MR and X-ray segmentation than ultrasound. Unlike these methods, in this paper we present an ultrasound-specific segmentation approach that first decorrelates the image, and then performs segmentation on the whitened result using statistical region-based active contours. In particular, we design a gradient ascent flow that evolves the active contours to maximize a log likelihood functional based on the Fisher-Tippett distribution. We present experimental results that demonstrate the effectiveness of our method.

1 Introduction

Ultrasound is one of the most commonly used medical imaging modalities. Compared to other modalities such as X-ray, MR, and PET, ultrasound scanning has many advantages, as it is fast, portable, relatively low cost, and presents virtually no risk to the patient.

However, the primary limitation of ultrasound is image quality. Ultrasound images are corrupted by speckle noise, an interference pattern resulting from the coherent accumulation of random scattering in a resolution cell of the ultrasound beam. While the texture of the speckle does not correspond to any underlying structure, the local brightness of the speckle pattern is related to the local echogenicity of the underlying scatterers. The speckle appears as a spatially correlated noise pattern and has a detrimental effect on the image quality and interpretability.

Since the speckle obfuscates the structures of interest, it also poses a difficult challenge to segmentation algorithms. While several authors in the past have presented ultrasound segmentation methods [2, 3, 10, 14, 18], previous approaches have not fully considered the statistical nature of the speckle noise [20]. Many methods assume that the pixels in an ultrasound image are spatially uncorrelated and the intensities follow a Gaussian distribution. Such assumptions render the problem more tractable, but are oversimplifications that result in generic segmentation approaches that are actually more suitable to other imaging modalities than ultrasound. Exceptions to this Gaussian assumption include [1], which presents a method to segment SAR images using Gamma distributions, [18], which considers Rayleigh distributions, and [13, 19], which utilize non-parametric densities in an information theoretic framework. However, none of these methods addresses the correlation of the noise.

This work is inspired by Chesnaud et al. [5], who present an algorithm for segmentation of images whose intensity can be described by an exponential distribution that evolves a deformable polygon. Recently, [18] extended this work, for the case of Rayleigh distributions, to a continuous curve representation modeled with level sets. However, neither of these methods considers the spatial correlation of the data. Furthermore, it appears that these techniques apply the Rayleigh distribution segmentation approach to the log magnitude image.

1.1 Our Contribution

In this paper we present an ultrasound-specific segmentation approach that address both the spatial correlation of the speckle data as well as its intensity distribution. The approach relies on two steps. First, we decorrelate the ultrasound image by applying a whitening filter. This filter-

ing operation is designed to remove the spatial correlation of the data, while maintaining its diagnostic information. Then, we apply a statistical region-based flow based on the Fisher-Tippett (FT) distribution, proposed [16, 8] as a model for image intensities observed in the log-compressed ultrasound image, for evolution of an active contour to relevant structures. This flow propagates the active contour using statistical measures of the data inside and outside the active contour. To our knowledge, this is the first paper to address the segmentation of decorrelated images. Another original contribution is the derivation and use of an active contour to segment images modeled by Fisher-Tippett distributions, which we argue are appropriate for the log-compressed image. We model the curve using a level set approach, which provides sub-pixel resolution and easily handles topological changes. Experimental results demonstrate that this more accurate modeling of the speckle noise, both in terms of its spatial correlation and intensity distribution, produces better segmentation results. The overall system block diagram is shown in Figure 1.

2 Statistical Modeling of Ultrasound Speckle

Before describing our decorrelation and segmentation method, it is worthwhile to review the statistics of speckle in an ultrasound image. Due to space limitations this review is very brief; further details can be found in [20, 8, 16, 11].

As shown in Figure 1, in-phase/quadrature (IQ) images are obtained by applying frequency demodulation to standard radio-frequency (RF) data from the transducer. This B-mode IQ image is complex and is the input to our approach.

2.1 Intensity Distribution

Speckle noise is an interference pattern resulting from the coherent accumulation of random scattering in a resolution cell of the ultrasound beam. In the case of fully formed speckle, which is typically assumed when the number of scatters per cell is greater than ten [8], it is assumed that each scatterer contributes an independent random complex component, resulting in a random walk in the complex plane. If one applies the central limit theorem to the random walk, one observes that the distribution is a Gaussian pdf in the complex plane, i.e.,

$$p_Z(z) = \frac{1}{2\pi\sigma^2} e^{-|z|^2/(2\sigma^2)} \tag{1}$$

where z is complex. This PDF models the data in the IQ image. To produce a real image for display, envelope detection is performed by taking the magnitude of the IQ image. It is fairly straightforward to show that under this transformation, the distribution in the magnitude image is Rayleigh [11], i.e.,

$$p_X(x) = \frac{x}{\sigma^2} e^{-x^2/(2\sigma^2)}, \tag{2}$$

where x is real. Typically, the magnitude image has a large dynamic range, and therefore the standard is to log-compress the image to produce an image suitable for display. Taking the log, i.e., Y = log(X), one can derive the distribution in the log image,

$$p_Y(y) = p_X(x) \left| \frac{dy}{dx} \right|^{-1}, \tag{3}$$

using $dy/dx = 1/x = e^{-y}$, to get

$$p_Y(y) = 2\exp([2y - \ln(2\sigma^2)] - \exp([2y - \ln(2\sigma^2)]), \tag{4}$$

which is a doubly exponential distribution that has the form of a Fisher-Tippett distribution. This distribution therefore is the theoretical model for the image intensities for fully formed speckle in the log-compressed IQ image.

To verify these theoretical models, we analyzed a real ultrasound image taken of a lesion phantom (ATS Laboratories Inc, Model 539), shown in Figure 2. We selected an image region (indicated by a white box) corresponding to the "soft tissue," where primary variation in the image intensity is due the speckle. The magnitude of the IQ image is shown in (a); notice the dark appearance resulting from the large dynamic range of the intensities. We show the histogram of the magnitude IQ image in (b), and fit the histogram to a Gaussian distribution, which does not accurately represent the distribution, with a mean square error (MSE) of 13,120. In (c) we fit the histogram of the magnitude IQ image to a Rayleigh distribution, which is a much more accurate representation, resulting in a MSE of 3961, which is 69.8% less than that of the Gaussian fit.

The log-compressed image is shown in (d) of Figure 2, which is a typical presentation of an ultrasound image. As before, we selected a region of pixels in the image and fit a Gaussian distribution to the histogram as shown in (e). Notice that a Gaussian distribution is similarly inaccurate for modeling this asymmetric histogram, with a MSE for this fit of 14,770. In contrast, in (f) we fit a Fisher-Tippett distribution, which very accurately models the intensity distribution, with a MSE of 3938, which is 73.3% less than that of the Gaussian fit. All distributions in this paper were optimally fit using analytic methods. Similar results were found for other soft tissue regions in the image.

From this analysis we conclude that the Rayleigh distribution is a good choice for the magnitude image, and the Fisher-Tippett distribution is preferred for the log magnitude image. We also note that application of the Rayleigh distribution to the log-compressed IQ image is not ideal,

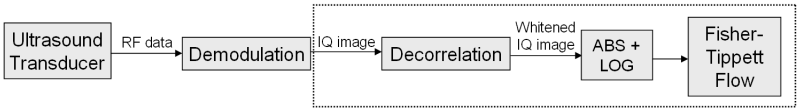

Figure 1. Block diagram. The ultrasound imaging system produces an IQ image, which is the input provided to our approach, which appears within the dotted rectangle.

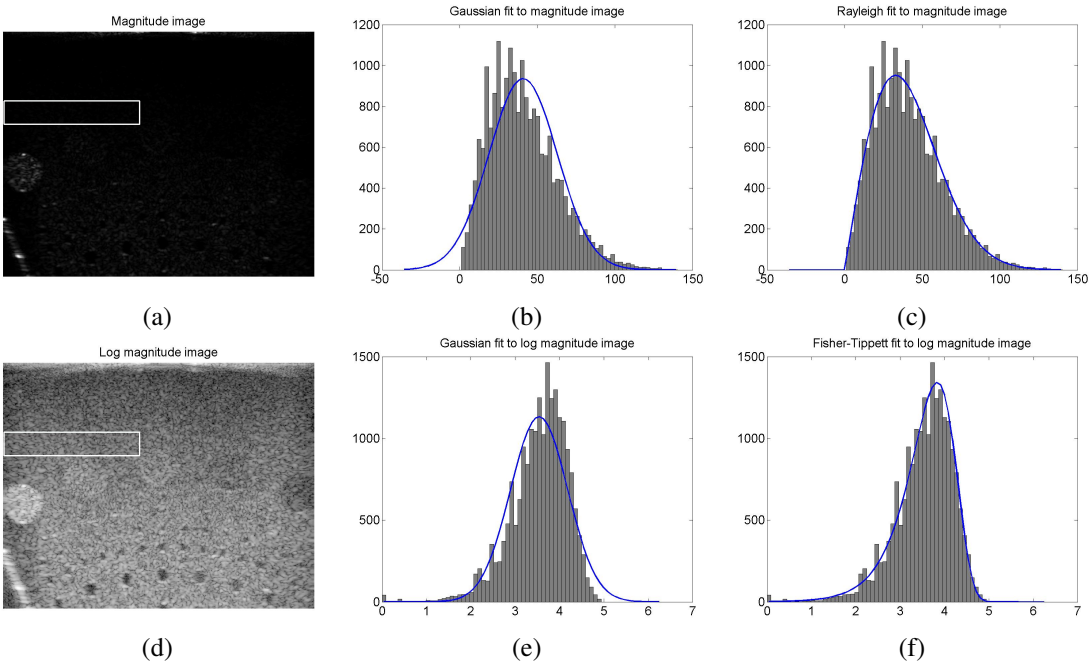

Figure 2. Using Rayleigh and Fisher-Tippett distributions to model ultrasound image intensities in the magnitude IQ (top row) and log magnitude IQ images (bottom row), respectively.

as the Rayleigh and Fisher-Tippett distributions are notably different. Among other differences, the long tail of the Rayleigh distribution is located to the right of the peak, while in the Fisher-Tippett distribution, the long tail is found on the left side of the peak. In Section 4 we will derive a variational flow for region-based segmentation based on the Fisher-Tippett distribution.

We should note that non-Rayleigh scattering can occur in the magnitude image when the number of scatterers is low, their spatial locations are not independent, or the scattering is not diffuse. In these cases, numerous distributions for modeling the ultrasound image intensities have been proposed, including the Homodyned K, Rice, Nakagami, Weibull, Generalized Gaussian, and Rician-Inverse Gaussian (RiIG) distributions [9, 17]. It is beyond the scope of this paper to consider all these cases, and how these distributions transform upon taking the log of the image. However, in [17], the authors argue that the Fisher-Tippett distribution is appropriate for fully formed speckle and is a reasonable approximation in these other cases.

2.2 Spatial Correlation

At this point we have characterized the image intensity distribution, but we have not yet addressed its spatial correlation, which renders ultrasound as arguably one of the more challenging medical imaging modalities with which to work. To understand this spatial correlation, we assume a standard image formation model where the backscattered signal and the tissue reflectivity function obey a simple relationship based on linear systems theory. Under the assumption of linear wave propagation and weak scattering, the IQ image is considered to be the result of the convolution of the point spread function (PSF) of the imaging system with

the tissue reflectivity function, i.e.,

$$g(x,y) = f(x,y) * h(x,y) + u(x,y) \tag{5}$$

where $g(x,y)$, $f(x,y)$, and $h(x,y)$ denote the IQ image, the tissue reflectivity function, and the PSF, respectively. The additive term $u(x,y)$ describes measurement noise and physical phenomena that are not covered by the convolution model. In the equation above, the received IQ image $g(x,y)$ is considered to be a filtered version of the true reflectivity function $f(x,y)$. The spatial extent of the PSF is dependent upon the size of the aperture as well as the frequency of the ultrasound imaging. Since the PSF is essentially a finite bandwidth low-pass filter, it imparts non-negligible spatial correlation to the IQ image. The correlation can be measured experimentally by calculating the half-bandwidth of the autocorrelation function of the log magnitude IQ image, as shown in Figure 3. This function has a notable bandwidth indicating the spatial correlation of the data; estimated half-bandwidth sizes are 2.76 and 4.49 pixels, respectively. Clearly, speckle noise in any real imaging situation has significant spatial correlation that should be addressed by an ultrasound segmentation method. Thus, we can improve upon previous algorithms that assume that the speckle is a white noise process. To address the spatial correlation, we first transform the IQ image using a whitening filter that decorrelates the data, resulting in another IQ image with pixels that correlate less than the original image. This procedure is described next.

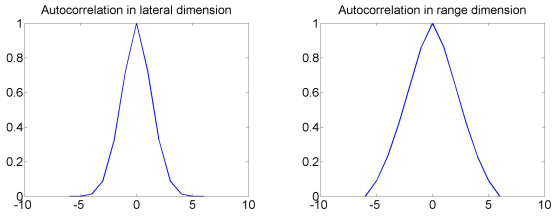

(a) (b)

Figure 3. The autocorrelation function of the selected region from Figure 2 is shown in the lateral (horizontal) dimension in (a) and the range (vertical) direction (b).

3 Decorrelation using outlier-resistent wavelet denoising

We perform whitening of speckled images [12] by the use of a decorrelation procedure proposed in [17], which we briefly review in this section.

It is possible to suppress the correlation by "undoing" the effect of the PSF through the process of deconvolution. As the PSF usually is not available a priori when dealing with tissue images, the deconvolution must be blind. Transferring the image formation model above to the frequency domain and applying log-transformation to the magnitudes of its components, one obtains

$$G(\omega_1,\omega_2) = H(\omega_1,\omega_2) + F(\omega_1,\omega_2) \tag{6}$$

where $G(\omega_1,\omega_2)$, $F(\omega_1,\omega_2)$, and $H(\omega_1,\omega_2)$ denote the log-magnitude of the Fourier transforms of the IQ image, the tissue reflectivity function, and the complex PSF, respectively. For simplicity, the additive noise term from (5) is ignored. The log-spectrum of $H(\omega_1,\omega_2)$ can be calculated by first removing the outliers from $G(\omega_1,\omega_2)$, in effect reducing the tail of the distribution, and by then estimating the PSF by means of wavelet denoising.

H is estimated as follows. First, an outlier shrinkage step computes the robust residuals R of G, with

$$R(x,y) = \text{sign}\left(\Delta G(x,y)\right) \cdot \left(|\Delta G(x,y)| - \lambda\right)_+, \tag{7}$$

where ΔG is the difference between G and its median-filtered version and λ is a predefined threshold, and the operator $(x)_+$ returns x if $x > 0$ and 0 otherwise. The median filter used is of size 3×3 and λ is dynamically adapted to a level such that a certain percentage (95%) of the differences ΔG is preserved. Next, the signal $G - R$ can be filtered to get an estimation of the PSF log spectrum $H(\omega_1,\omega_2)$. For this purpose, wavelet denoising [7] with a separable wavelet transform [15] based on the nearly symmetric wavelet of Daubechies [6] having six vanishing moments is used.

Once an estimate of $H(\omega_1,\omega_2)$ is computed, the PSF spectrum magnitude is given by $S(\omega_1,\omega_2) = e^{H(\omega_1,\omega_2)}$. An equalized IQ image $\tilde{g}$ is then obtained by applying the classical deconvolution filter as in [12]:

$$\tilde{g}(x,y) = DFT^{-1}\left\{\frac{DFT\{g(x,y)\}}{\left[|S(\omega_1,\omega_2)|^2 + \epsilon\right]^{1/2}}\right\},$$

with $0 < \epsilon \ll 1$.

The noise in the decorrelated image has significantly less spatial correlation, as depicted in Figure 4; the half-bandwidth size has decreased to 1.4 pixels in the lateral dimension and 2.5 in the range dimension. Visually, this decorrelated image appears to have a higher spatial resolution as finer details become apparent.

It is natural to wonder if the decorrelation affects the intensity distributions, i.e., if the Rayleigh and Fisher-Tippett distribution models still apply to magnitude and log magnitude decorrelated IQ images, respectively. To check, we repeated the previous experiment of fitting Rayleigh and Fisher-Tippett distributions to histograms formed over the same soft tissue region in the phantom image. As demonstrated in Figure 5, the decorrelation does not significantly affect the distribution, so we infer that the models still hold.

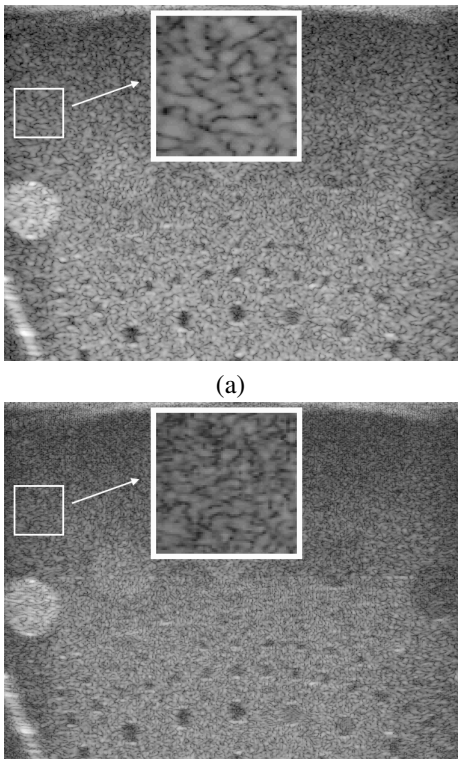

(a) (b)

Figure 4. Decorrelation decreases speckle size. Original image (a) and decorrelated image (b).

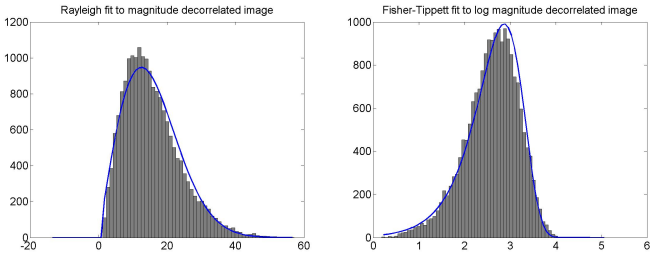

(a) (b)

Figure 5. Previous distributions apply to the decorrelated image. The Rayleigh fit to the magnitude IQ decorrelated image is shown in (a), and the Fisher-Tippett fit to the log magnitude decorrelated IQ image is shown in (b).

4 Maximum Likelihood Fisher-Tippett Segmentation

We now derive a flow for maximum likelihood region-based segmentation of an image described by Fisher-Tippett distributions, which we will apply to the log magnitude IQ image. In a spirit similar to [4], we will evolve a contour embedded as the zero level set of a higher dimensional function based on statistical measures computed both inside and outside the contour. We begin by deriving the maximum likelihood Fisher-Tippett estimator for a collection of samples.

4.1 Maximum likelihood Fisher-Tippett estimator

Let $I(x,y)$ denote a pixel intensity in the decorrelated log magnitude IQ image at the location (x,y). As stated previously, the Fisher-Tippett PDF for a pixel's intensity can be written as

$$p(I(x,y)) = 2e^{\left(2I(x,y)-\ln(2\sigma^2)-e^{2I(x,y)-\ln(2\sigma^2)}\right)}, \quad (8)$$

where σ^2 denotes the Fisher-Tippett parameter of the reflectivity samples. For a region Ω in the image, the log likelihood can then be expressed as

$$\ell = \int_\Omega \left(\ln 2 + 2I(x,y) - \ln(2\sigma^2) - e^{2I(x,y)-\ln(2\sigma^2)}\right) dxdy. \quad (9)$$

Next, we find an expression for σ^2 that is the maximum likelihood estimator of the FT distribution, by taking the derivative of ℓ and setting the expression equal to zero,

$$\frac{\partial \ell}{\partial \sigma} = \int_\Omega \left(-\frac{4\sigma}{2\sigma^2} + \left(e^{2I(x,y)-\ln(2\sigma^2)}\right)\frac{4\sigma}{2\sigma^2}\right) dxdy = 0. \quad (10)$$

Solving for σ^2 gives

$$\sigma^2 = \frac{1}{2}\frac{\int_\Omega e^{2I(x,y)}dxdy}{\int_\Omega dxdy}. \quad (11)$$

Thus, given a region Ω with area given by $\int_\Omega dxdy$, we can compute the maximum likelihood value of the Fisher-Tippett distribution from the image intensities in the region. We will do this to estimate the Fisher-Tippett parameter σ^2 both inside and outside the active contour.

4.2 Fisher-Tippett flow

We would like to deform a curve C in order to achieve a maximum likelihood segmentation of the data. Since the log function is monotonic, we can equivalently maximize the log likelihood [5, 18], using the probability inside and outside the curve, P_i and P_o, respectively, as

$$E = \log P_i + \log P_o + \text{regularization} \quad (12)$$

$$= A_i \log\left(\frac{1}{2A_i}\int_{\Omega_i} e^{2I(x,y)}dxdy\right) \quad (13)$$

$$+A_o \log\left(\frac{1}{2A_o}\int_{\Omega_i} e^{2I(x,y)}dxdy\right) + \alpha\int_C ds,$$

where Ω_i and Ω_o are a regions inside and outside the curve, respectively, and $A_i = \int_{\Omega_i} dxdy$ and $A_o = \int_{\Omega_o} dxdy$ are the areas inside and outside the curve, respectively, and the last term is a penalty on arc length designed to keep the curve smooth.

Next, we take the first variation of this energy functional E in order to derive the minimizing flow. Due to page constraints we do not provide the full derivation here; however, the derivation takes a similar form to that of the Rayleigh distribution that appears in [18]. The Euler-Lagrange equations result in the curve evolution,

$$\frac{\partial C}{\partial t} = \Big(\log\sigma_i^2 - \log\sigma_o^2 + \frac{\frac{1}{2}e^{2I} - \sigma_i^2}{\sigma_i^2} - \frac{\frac{1}{2}e^{2I} - \sigma_o^2}{\sigma_o^2} + \alpha\kappa\Big)\mathbf{N}, \quad (14)$$

where κ is the curvature and $\mathbf{N}$ is the normal to the curve.

4.3 Implementation

The curve evolution in Equation 14 is totally general in that it applies to any closed contour representation, be it a spline, polygon, etc. The method requires an initial contour, which in this paper is a small square positioned by the user. Then, we compute the maximum likelihood FT parameters σ_i^2 and σ_o^2 inside and outside the contour using the method described in Section 4.1. Then, we move each point on the contour along its normal direction using Equation 14. We choose to implement the technique using level set methods, which provide subpixel resolution and easily accommodate topological changes of the contour.

5 Results

In this section we present results demonstrating segmentations of quite challenging images.

In Figure 6 we present segmentation results using synthetically generated data consisting of darker targets on a lighter background. In each experiment we seed the segmentation with a small square in the upper left part of the right lower circular target. In (a) and (b), we show the Rayleigh and Fisher-Tippett flows, respectively, applied to the log magnitude IQ data. The Rayleigh flow does not perform well, getting trapped in an undesirable local minimum. The Fisher-Tippett flow performs much better, but the speckle correlation prevents the segmentation from reaching all parts of the circle. In (c) and (d), we show the Rayleigh and Fisher-Tippett flows, respectively, applied to the decorrelated image. Here, the best results are observed for the Fisher-Tippett flow, which successfully segments the target. For this synthetic data, we have the ground truth area, which is 7854 units. The areas inside the contours computed from the segmentations were 763 for (a), 6393 for (b), 7548 for (c), and 7815 for (d). Similar results we obtained for the other shapes in the image. We can conclude that for this experiment, the Fisher-Tippett flow applied to the decorrelated image produces the best result, both visually and quantitatively.

In Figure 7 we show a result for the segmentation of the lesion phantom for the rightmost faint circular structure that simulates a tumor. In (a) we show the result of applying the Rayleigh flow to the original log magnitude IQ image. This segmentation gets stuck due to the speckle and the inaccurate intensity model. In (b) we show the result of applying the Fisher-Tippett flow to the decorrelated log magnitude image. This segmentation results in a more circular shape that covers the entire area of the object. Thus, as with the synthetic data, the best results occur for the Fisher-Tippett flow on the decorrelated log magnitude image.

In Figure 8 we present segmentation results using the Rayleigh and Fisher-Tippett flows applied to a log magnitude IQ image and a decorrelated log magnitude IQ image of a human carotid artery. In each example we initialized the segmentation with a small rectangular seed on the left side of the artery. In (a) and (b), we show the result of the Rayleigh flow and Fisher-Tippett flow, respectively. Neither achieves a successful result due to the correlation of the speckle, as well as the difficulty due to poor separation of the statistics inside and outside the contour resulting from the dark pixels in the lower half of the image. In (c) and (d) we show the Rayleigh and Fisher-Tippett flows applied to the decorrelated image. Due to an inaccurate modeling of the intensity distribution, Rayleigh flow still is unable to propagate the length of the artery. However, the Fisher-Tippett flow significantly outperforms the Rayleigh flow, as the former propagates the entire length of the artery, producing the best result. In (e) - (i) we repeat the previous experiment, this time cropping the image to its upper half. In this case, the statistics inside and outside the contour are better separated, so in this case all segmentations propagate the length of the artery. In (e) and (f), the correlation of the speckle results in an irregular shape that does not properly match the artery borders. In (g) and (h), better results are achieved for the decorrelated image, and due to its better modeling of the intensity distributions, the result for the Fisher-Tippett flow in (h) produces the best result.

6 Conclusion

In this paper we present ultrasound-specific methods for image segmentation. Speckle noise can be difficult to handle since it exhibits significant spatial correlation and does not generally follow a Gaussian distribution. Our method

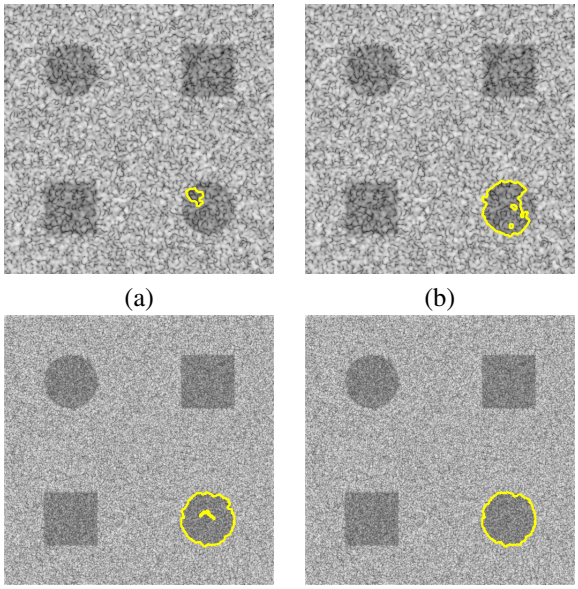

Figure 6. Segmentation of synthetically generated data. Top row: Rayleigh (a) and Fisher-Tippett flows applied to original log magnitude image. Bottom row: Rayleigh (c) and Fisher-Tippett flows (d) applied to decorrelated image.

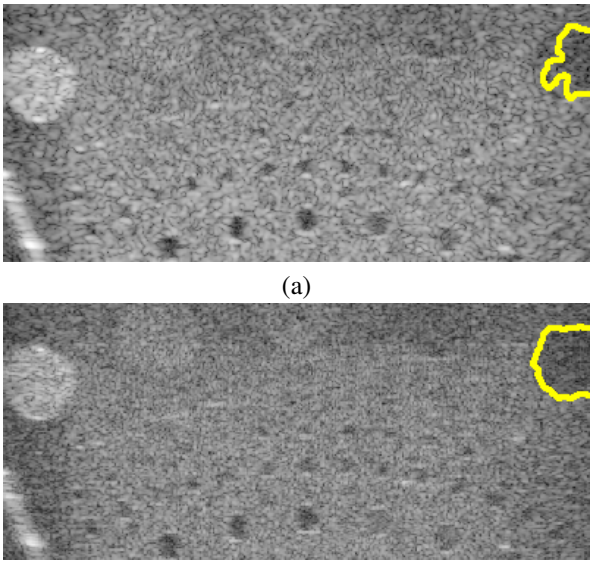

Figure 7. Segmentation of a lesion phantom. In (a), the Rayleigh flow is applied to the original magnitude IQ image, and in (b) the Fisher-Tippett flow is applied to the log magnitude IQ image.

first decorrelates the ultrasound image using a whitening filter. We then perform maximum likelihood segmentation using region-based active contours and the Fisher-Tippett distribution model. In all our experiments, we observed the best results when we applied the Fisher-Tippett flow on the decorrelated images.

While more comprehensive validation of the algorithm is required, from our experimental results we conclude that the combined decorrelation and statistical region-based active contour results in improved segmentation results. For future work we are interested in validating the method with more IQ ultrasound data, and applying the method to clinical applications like tumor segmentation. Furthermore, we believe the theory underlying this paper will be useful in other applications, such as filtering, tracking, and registration; we plan on investigating these topics in the future.

7 Acknowledgements

The authors would like to thank Dr. Bimba Rao of Siemens Medical Solutions, Ultrasound Division for her assistance with IQ data acquisition.

References

[1] I. Ayed, A. Mitiche, and Z. Belhadj. Multiregion Level-Set Partitioning of Synthetic Aperture Radar Images. *IEEE Trans. on Patt. Anal. and Mach. Intel.*, 27(5):793–800, 2005.

[2] B. Baillard and C. Barillot. Robust 3D Segmentation of Anatomical Structures with Level Sets. In *Proc. MICCAI*, pages 236–245, 2000.

[3] D. Boukerroui, O. Basset, A. Baskurt, and G. Gimenez. A Multiparametric and Multiresolution Segmentation Algorithm of 3-D Ultrasonic Data. *IEEE Trans. on Ultrasonics, Ferroelectrics, and Freq. Control*, 48(1):64–77, 2001.

[4] T. Chan and L. Vese. Active Contours Without Edges. *IEEE Trans. on Image Processing*, 10(2):266–277, 2001.

[5] C. Chesnaud, P. Réfrégier, and V. Boulet. Statistical Region Snake-Based Segmentation Adapted to Different Physical Noise Models. *IEEE Transactions on Pattern Analysis and Machine Intelligence*, 21(11):1145–1157, 1999.

[6] I. Daubechies. Ten Lectures on Wavelets. In *CBMS-NSF Regional Conf. Series in App. Math.*, volume 91, 1992.

[7] D. L. Donoho. De-noising by Soft-Thresholding. *IEEE Trans. on Information Theory*, 41(3):613–627, 1995.

[8] V. Dutt and J. Greenleaf. Statistics of the Log-Compressed Envelope. *Journal of the Acoustical Society of America*, 99(6):3817–3825, 1996.

[9] T. Eltoft. Modeling the amplitude statistics of ultrasonic images. *IEEE Trans. on Med. Img.*, 25(2):229–240, 2006.

[10] M. M. Fernández and C. Alberola-López. Contour Detection of Human Kidneys from Ultrasound Images using Markov

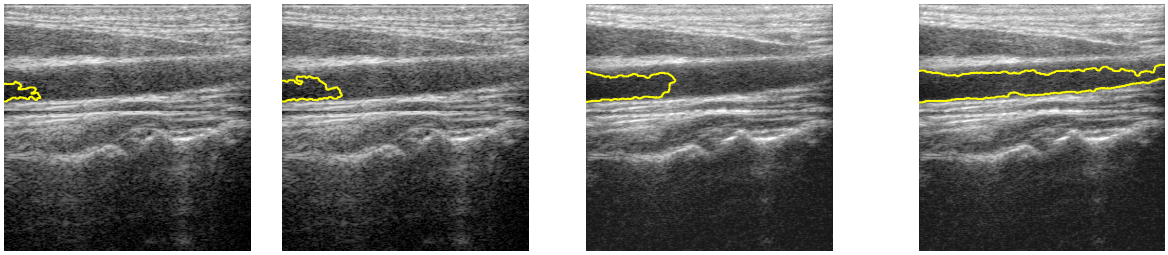

(a) Log Mag IQ Image Rayleigh flow (b) Log Mag IQ Image Fisher-Tippett flow (c) Log Mag Dec. IQ Image Rayleigh flow (d) Log Mag Dec. IQ Image Fisher-Tippett flow

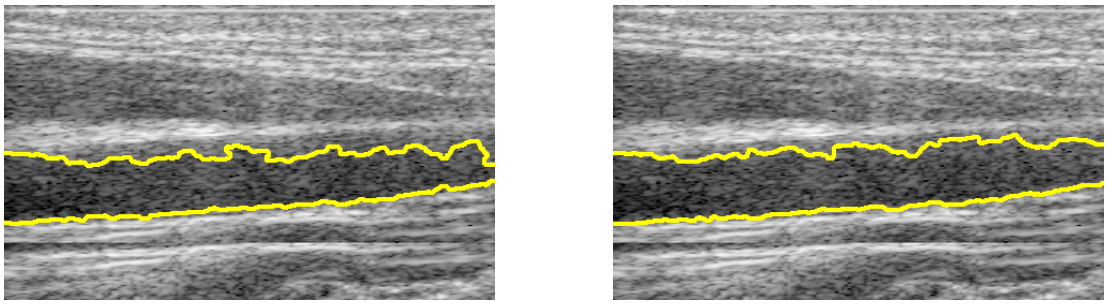

(e) Log Mag IQ Image, Rayleigh flow (f) Log Mag IQ Image, Fisher-Tippett flow

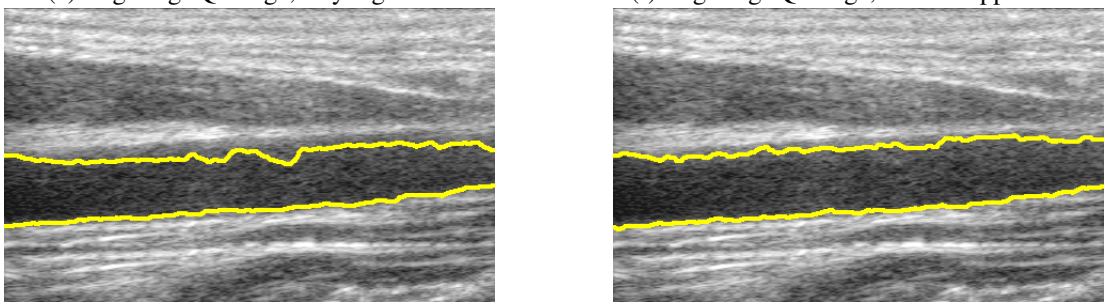

(g) Log Mag Decorrelated IQ Image, Rayleigh flow (h) Log Mag Decorrelated IQ Image, Fisher-Tippett flow

Figure 8. Carotid artery segmentation. Results (a) - (d) show the first experiment on the full image, while (e) - (h) show the second experiment on the cropped image. For both experiments, the best results are obtained when the Fisher-Tippett flow is applied to the decorrelated image.

Random Fields and Active Contours. *Medical Image Analysis*, 9(1):1–23, 2005.

[11] J. Goodman. *Speckle Phenomena: Theory and Applications*. Work in Progress, first edition, 2005.

[12] D. Iraca, L. Landini, and L. Verrazzani. Power Spectrum Equalization for Ultrasonic Image Restoration. *IEEE Trans. on Ultrasonics, Ferroelectrics, and Frequency Control*, 36(2):216–222, 1989.

[13] J. Kim, J. W. Fisher, A. Yezzi, M. Cetin, and A. Willsky. A Nonparametric Statistical Method for Image Segmentation Using Information Theory and Curve Evolution. *IEEE Trans. on Image Processing*, 14(10):1486–1502, 2005.

[14] N. Lin, W. Yu, and J. Duncan. Combinative Multi-Scale Level Set Framework for Echocardiographic Image Segmentation. *Medical Image Analysis*, 7(4):529–537, 2003.

[15] S. Mallat. *A Wavelet Tour of Signal Processing*. Academic Press, New York, 1998.

[16] O. Michailovich and D. Adam. Robust Estimation of Ultrasound Pulses Using Outlier-Resistant De-Noising. *IEEE Trans. on Medical Imaging*, 22(3):368–392, 2003.

[17] O. Michailovich and A. Tannenbaum. Despeckling of Medical Ultrasound Images. *IEEE Trans. on Ultrasonic Ferroelectrics and Frequency Control*, 53(1):64–78, 2006.

[18] A. Sarti, C. Corsi, E. Mazzini, and C. Lamberti. Maximum Likelihood Segmentation of Ultrasound Images with Rayleigh Distribution. *IEEE Trans. on Ultrasonics, Ferroelectrics, and Freq. Control*, 52(6):947–960, 2005.

[19] G. Unal, A. Yezzi, and H. Krim. Information-theoretic active polygons for unsupervised texture segmentation. *The Intl. Journal of Computer Vision*, 62(3):199–220, 2005.

[20] R. Wagner, S. Smith, J. M. Sandrik, and H. Lopez. Statistics of Speckle in Ultrasound B-Scans. *IEEE Transactions on Sonics and Ultrasonics*, 30(3):156–163, 1983.